PHYSICAL REVIEW B VOLUME 13, NUMBER 12 15 JUNE 1976

Piezospectroscopic study of the Raman spectrum of cadmium sulfide*

R. J. Briggs and A. K. Ramdas
Department of Physics, Purdue University, West Lafayette, Indiana 47907

(Received 12 December 1975)

The effect of uniaxial stress on the one-phonon Raman lines of CdS having A_1, E_1, and E_2 symmetries are studied for compressive force $\vec{F}$, either along the a axis ($\hat{x}$) or the c axis ($\hat{z}$) and using a low-temperature stress cryostat. The scattering geometries chosen resulted in the phonon propagation direction $\vec{q}$ being either parallel or perpendicular to z; this in turn allowed the observation of pure E_1(TO), E_1(LO), A_1(TO), and A_1(LO) lines. For $\vec{F} \parallel \hat{x}$, the lines or their components shift linearly with stress. The E_2 line at 256 cm^{-1} splits into two clearly resolved components, the polarization features being consistent with the deformation-potential theory. The E_1(TO) and the E_1(LO) lines separate further, whereas the A_1(TO) and the A_1(LO) lines increase at the same rate. For $\vec{F} \parallel \hat{z}$, all the lines exhibit shifts linear in stress; the E_1(TO) and the E_1(LO) lines increase at the same rate, and the E_2 line at 256 cm^{-1} does not split. From the results for $\vec{F} \parallel \hat{x}$ and $\vec{F} \parallel \hat{z}$, the deformation-potential constants characterizing each line have been deduced. A comparison of the piezospectroscopy of the doubly degenerate E_1 line of CdS with that of the E lines of α-quartz is presented along with some new results for the latter. The LO overtones observed in $\bar{y}(zz)y$ geometry shift linearly for $\vec{F} \parallel \hat{z}$; the rates of shift increase linearly with increasing order. The magnitudes of these shifts suggest that all overtones are of E_1 nature.

I. INTRODUCTION

Cadmium sulfide (CdS), an important member of the II-VI semiconductors with the wurtzite structure, has been the subject of numerous optical investigations.[1] The energy gap, the exciton binding energies, and the symmetry of the band extrema have been deduced from a variety of optical experiments close to the absorption edge.[1-3] Polarized infrared reflectivity measurements[4-6] (reststrahlen) have given the positions of the transverse-optical (TO) phonons polarized parallel and perpendicular to the optic axis as well as the static and high-frequency dielectric constants; the corresponding longitudinal-optical (LO) phonons were deduced through the use of the Lydanne-Sachs-Teller relationship. Phonon-assisted transitions in luminescence near the band edge,[7] oscillatory intrinsic photoconductivity,[8] and the multiphonon infrared absorption[9] have yielded phonon energies at both zone center and zone boundary. It appears that no neutron scattering work has been done on this material because of its high neutron absorption.[10] Tell *et al.*[11] and Arguello *et al.*[12] have carried out a complete analysis of the one-phonon Raman spectrum. The multiphonon features observable in the work of Tell *et al.* have been interpreted by Nusimovici and Birman[13] on the basis of a lattice-dynamical calculation. One of the most striking features of the Raman spectrum of cadmium sulfide is the remarkable overtone series of the LO phonons.[14-16] By employing incident energies close to the band gap, the intensities of these overtones have been shown to increase up to six orders of magnitude[17] and as many as nine overtones have been observed.[14]

External perturbation has been utilized in the study of the Raman spectrum of cadmium sulfide. Shand *et al.*[18] have reported electric-field-induced scattering from the LO phonons. Under external magnetic field Damen and Shah[19] observed resonance enhancements of the 1LO and the 3LO overtone intensities and interpreted them as resonance effects associated with the Landau levels of the Γ_7 conduction and valence bands. Shifts of some of the Raman lines under hydrostatic stress have been reported by Mitra *et al.*[20] In this paper, we present the results of our investigation of the effect of uniaxial stress on both the one-phonon and the LO-overtone spectrum and interpret them in the light of the linear-deformation-potential theory.[21]

II. EXPERIMENTAL

A Jarrell-Ash double monochromator,[22] a cooled RCA C31034 or ITT FW130 photomultiplier[23] with the associated photon counting electronics, and a Coherent Radiation[24] (Model 52A) Ar$^+$ laser as well as a Spectra Physics[25] (Model 125) He-Ne laser constituted the Raman spectrometer used in the present investigation.[26] The excitation lines provided by these lasers allowed the use of exciting radiation either above or below the band gap of CdS. A right-angle scattering geometry was employed when experiments were performed with exciting radiation below the band gap whereas the "reflection" or "back scattering" technique was used for exciting radiation above the band gap. The accuracy of the positions of the Raman lines was improved by using calibration lines from a Nd-hollow-cathode lamp.[27] The spectra recorded were corrected for the polarization features of the instrumental function by using a Fresnel rhomb before the entrance slit in order to convert the "vertical" and "horizontal" polarizations to directions each at 45° to the horizontal scattering plane; thus the vertical and horizontal polarizations were treated equally by the double monochromator.[28] The stress cryostat used for the piezospectroscopic experiments and the procedure for sample mounting are described in Ref. 29.

The CdS specimens used in this investigation were cut from ultrahigh-purity, vapor-phase-grown single crystals obtained from Eagle-Picher.[30] The crystals were oriented with x-rays and cut in the form of parallelepipeds suitable for the uniaxial stress experiments. The orientations were confirmed using conoscopic figures in convergent monochromatic light. Two orientations were extensively used in this work: the first had its face normals along[31] $\hat{x}\|\vec{a}\|[2\bar{1}\bar{1}0]$, $\hat{y}\|[0\bar{1}10]$, and $\hat{z}\|\vec{c}\|[0001]$ and is called the "rectangular cut"; the second, called the "45° cut", had as its face normals x, y', and z' with y' and z' at $-45°$ and $+45°$ with respect to z in the yz plane.[32] After cutting to size, samples were ground with successively finer grits of carborundum powder and the desired faces polished on AB Microcloth using a 600-grit and finally a 3200-grit slurry.[33]

III. THEORY

A. Zero stress

Cadmium sulfide belongs to the C_{6v}^4 ($P6_3mc$) space-group symmetry with two formula units per primitive cell. Hence the zone-center optical phonons can be classified according to the irreducible representations of C_{6v} as follows: one totally symmetric (A_1); one doubly degenerate infrared and Raman active (E_1); two doubly degenerate active in Raman scattering only (E_2); and two antisymmetric with respect to the twofold and sixfold axes (B_1), "silent modes" inactive in both infrared absorption and Raman scattering (see Table I). For phonon propagation along $\vec{q}$ perpendicular to the optic axis, the long-range polarization field splits the E_1 phonon into an E_1(LO) and an E_1(TO) phonon whereas the A_1 phonon remains as A_1(TO). On the other hand, for $\vec{q}\|\vec{c}$, the E_1 phonon is unsplit and the long-range polarization field changes the A_1 to A_1(LO). For intermediate directions, one finds LO and TO phonons which are mixtures of A_1 and E_1.[12] In contrast to the infrared reststrahlen, Raman scattering allows a direct observation of both the TO and LO components. Also, the nonpolar E_2 modes are observable only in the Raman effect. Thus the first-order Raman spectrum permits an unambiguous determination of more phonons whose symmetries are identifiable from their distinguishable polarization features. The polarization characteristics can be deduced from the polarizability tensors for the phonons of A_1, E_1, and E_2 symmetries given in Table II referred to either the x,y,z or the x,y',z' axes.

B. Effect of uniaxial stress

The symmetry of the crystal under uniaxial compression is determined by the symmetry elements common to both the unstrained crystal and the strain ellipsoid.[34] The reduced symmetries as well as the commom symmetry elements for compressive force $\vec{F}$ along different crystallographic directions are listed in Table III.

We now consider the effect of uniaxial stress in terms of the linear deformation potential theory.[35] In this theory the perturbing potential is given by

$$V=\sum V_{ij}\epsilon_{ij}, \quad i,j=x,\ y,\ \text{or}\ z, \tag{1}$$

where the ϵ_{ij}'s are the components of the strain tensor and the V_{ij}'s are the deformation potentials. Both $\{V_{ij}\}$ and $\{\epsilon_{ij}\}$ are symmetric second-rank tensors. For CdS, the representation gen-

TABLE I. Character table and zone-center phonons of CdS. N_t, N_a, and N_o denote the total number, the number of acoustic, and the number of optical zone center phonons, respectively, belonging to each irreducible representation.

C_{6v}	E	$2C_6$	$2C_3$	C_2	$3\sigma_v$	$3\sigma_d$	N_t	N_a	N_o	ir active	Raman active
A_1	1	1	1	1	1	1	2	1	1	Yes	Yes
A_2	1	1	1	1	−1	−1	0	0	0	No	No
B_1	1	−1	1	−1	1	−1	2	0	2	No	No
B_2	1	−1	1	−1	−1	1	0	0	0	No	No
E_1	2	1	−1	−2	0	0	2	1	1	Yes	Yes
E_2	2	−1	−1	2	0	0	2	0	2	No	Yes

TABLE II. Polarizability tensors of the Raman-active modes of CdS for the "rectangular" and "45°" cuts.

	Rectangular cut: x, y, z	45° cut: x, y', z'
A_1	$\begin{pmatrix} p & 0 & 0 \\ 0 & p & 0 \\ 0 & 0 & q \end{pmatrix}$	$\begin{pmatrix} p & 0 & 0 \\ 0 & \frac{1}{2}(p+q) & \frac{1}{2}(p-q) \\ 0 & \frac{1}{2}(p-q) & \frac{1}{2}(p+q) \end{pmatrix}$
$E_1: -X$	$\begin{pmatrix} 0 & 0 & -s \\ 0 & 0 & 0 \\ -s & 0 & 0 \end{pmatrix}$	$\begin{pmatrix} 0 & s/\sqrt{2} & -s/\sqrt{2} \\ s/\sqrt{2} & 0 & 0 \\ -s/\sqrt{2} & 0 & 0 \end{pmatrix}$
$E_1: Y$	$\begin{pmatrix} 0 & 0 & 0 \\ 0 & 0 & s \\ 0 & s & 0 \end{pmatrix}$	$\begin{pmatrix} 0 & 0 & 0 \\ 0 & -s & 0 \\ 0 & 0 & s \end{pmatrix}$
$E_2: f_\alpha$	$\begin{pmatrix} r & 0 & 0 \\ 0 & -r & 0 \\ 0 & 0 & 0 \end{pmatrix}$	$\begin{pmatrix} r & 0 & 0 \\ 0 & -\frac{1}{2}r & -\frac{1}{2}r \\ 0 & -\frac{1}{2}r & -\frac{1}{2}r \end{pmatrix}$
$E_2: f_\beta$	$\begin{pmatrix} 0 & -r & 0 \\ -r & 0 & 0 \\ 0 & 0 & 0 \end{pmatrix}$	$\begin{pmatrix} 0 & -r/\sqrt{2} & -r/\sqrt{2} \\ -r/\sqrt{2} & 0 & 0 \\ -r/\sqrt{2} & 0 & 0 \end{pmatrix}$

erated by $\{V_{ij}\}$ is $\Gamma_V = 2A_1 + E_1 + E_2$. Hence the components of $\{V_{ij}\}$ can be grouped as follows:

$$\begin{aligned} V = {} & \tfrac{1}{2}(V_{xx} + V_{yy})(\epsilon_{xx} + \epsilon_{yy}) + V_{zz}\epsilon_{zz} \\ & + 2[(V_{yz}\epsilon_{yz}) + (-V_{zx})(-\epsilon_{zx})] \\ & + \tfrac{1}{2}[(V_{xx} - V_{yy})(\epsilon_{xx} - \epsilon_{yy}) \\ & + (-2V_{xy})(-2\epsilon_{xy})]. \end{aligned} \tag{2}$$

In Eq. (2), $(V_{xx} + V_{yy})$ and V_{zz} belong to A_1, V_{yz} and $-V_{zx}$ belong to E_1, and $(V_{xx} - V_{yy})$ and $-2V_{xy}$ belong to E_2 as can be seen from the basis functions appropriate for the representations A_1, E_1, and E_2 of C_{6v} listed in Table IV. Thus, under stress the energy of a state belonging to A_1 will shift by

$$\tfrac{1}{2}\langle A_1 | V_{xx} + V_{yy} | A_1\rangle (\epsilon_{xx} + \epsilon_{yy}) + \langle A_1 | V_{zz} | A_1 \rangle \epsilon_{zz},$$

since the remaining terms vanish from the orthogonality theorem. The energy shift of the A_1 state is therefore

$$\Delta E_{A_1} = a_{A_1}(\epsilon_{xx} + \epsilon_{yy}) + b_{A_1}\epsilon_{zz}, \tag{3}$$

where $a_{A_1} = \frac{1}{2}\langle A_1 | V_{xx} + V_{yy} | A_1\rangle$ and $b_{A_1} = \langle A_1 | V_{zz} | A_1\rangle$ are the deformation potential constants. For the calculation of the matrix elements of V for the doubly degenerate E_1 and E_2 modes we need the decomposition of the products of the basis functions of C_{6v} which are given in Table V. Using symmetry arguments, the secular equation for an E_1 mode can be expressed in terms of three deformation-potential constants a_{E_1}, b_{E_1}, and c_{E_1} as follows:

TABLE III. Symmetry reduction for uniaxial stress along various crystallographic directions. The symmetry elements are referred to the x, y, z coordinate system and the axes in the planes are explicitly indicated within parenthesis.

Direction of force	Symmetry	Common elements
$\vec{F} \parallel \hat{z}$	C_{6v}	all
$\vec{F} \parallel \hat{x}$	C_{2v}	$C_2(z), \sigma_d(xz), \sigma_v(yz)$
$\vec{F} \parallel \hat{y}$	C_{2v}	$C_2(z), \sigma_d(xz), \sigma_v(yz)$
$\vec{F}$ in xz plane	C_s	$\sigma_d(xz)$
$\vec{F}$ in yz plane	C_s	$\sigma_v(yz)$
$\vec{F}$ in xy plane	C_2	$C_2(z)$

$$\begin{vmatrix} a_{E_1}(\epsilon_{xx}+\epsilon_{yy})+b_{E_1}\epsilon_{zz}+c_{E_1}(\epsilon_{xx}-\epsilon_{yy})-\Delta E & 2c_{E_1}\epsilon_{xy} \\ 2c_{E_1}\epsilon_{xy} & a_{E_1}(\epsilon_{xx}+\epsilon_{yy})+b_{E_1}\epsilon_{zz}-c_{E_1}(\epsilon_{xx}-\epsilon_{yy})-\Delta E \end{vmatrix}=0, \tag{4}$$

where

$$a_{E_1}=\tfrac{1}{4}\langle f_0 | V_{xx}+V_{yy}\rangle, \quad b_{E_1}=\tfrac{1}{2}\langle f_0 | V_{zz}\rangle, \tag{5}$$

and

$$c_{E_1}=\tfrac{1}{4}\langle f_\alpha | V_{xx}-V_{yy}\rangle=\tfrac{1}{4}\langle f_\beta | -2V_{xy}\rangle .$$

The resulting eigenvalues are

$$\Delta E_{E_1}=a_{E_1}(\epsilon_{xx}+\epsilon_{yy})+b_{E_1}\epsilon_{zz} \pm c_{E_1}[(\epsilon_{xx}-\epsilon_{yy})^2+4\epsilon_{xy}^2]^{1/2}. \tag{6}$$

For $\vec{F}\|\hat{x}$ or $\vec{F}\|\hat{z}$ the corresponding eigenfunctions are still Y and $-X$. They retain the distinct polarizability tensors given in Table II, even when referred to the "45° cut." Hence each component can be identified and the sign of the constant c_{E_1}, as defined, can be determined.

The secular equation for each E_2 mode is the same as Eq. (4) except that the three new deformation-potential constants are

$$a_{E_2}=\tfrac{1}{4}\langle f_0' | V_{xx}+V_{yy}\rangle, \quad b_{E_2}=\tfrac{1}{2}\langle f_0' | V_{zz}\rangle, \quad c_{E_2}=\tfrac{1}{4}\langle f_\alpha' | V_{xx}-V_{yy}\rangle=\tfrac{1}{4}\langle f_\beta' | -2V_{xy}\rangle, \tag{7}$$

and the two resulting eigenvalues are

$$\Delta E_{E_2}=a_{E_2}(\epsilon_{xx}+\epsilon_{yy})+b_{E_2}\epsilon_{zz} \pm c_{E_2}[(\epsilon_{xx}-\epsilon_{yy})^2+4\epsilon_{xy}^2]^{1/2}. \tag{8}$$

For $\vec{F}\|\hat{x}$ or $\vec{F}\|\hat{z}$ the eigenfunctions remain as f_α and f_β, and also retain their distinct polarizability tensors given in Table II.

For CdS, the components of the strain tensor $\{\epsilon_{ij}\}$ are related to the components of the stress tensor $\{\sigma_{ij}\}$ through the elastic compliance constants s_{ij} as given below, when referred to the xyz axes[31,36]:

$$\begin{pmatrix} \epsilon_{xx} \\ \epsilon_{yy} \\ \epsilon_{zz} \\ 2\epsilon_{yz} \\ 2\epsilon_{zx} \\ 2\epsilon_{xy} \end{pmatrix} = \begin{pmatrix} s_{11} & s_{12} & s_{13} & 0 & 0 & 0 \\ s_{12} & s_{11} & s_{13} & 0 & 0 & 0 \\ s_{13} & s_{13} & s_{33} & 0 & 0 & 0 \\ 0 & 0 & 0 & s_{44} & 0 & 0 \\ 0 & 0 & 0 & 0 & s_{44} & 0 \\ 0 & 0 & 0 & 0 & 0 & 2(s_{11}-s_{12}) \end{pmatrix} \begin{pmatrix} \sigma_{xx} \\ \sigma_{yy} \\ \sigma_{zz} \\ \sigma_{yz} \\ \sigma_{zx} \\ \sigma_{xy} \end{pmatrix} \tag{9}$$

TABLE IV. Basis functions for irreducible representations of C_{6v}.

Representation	Basis functions
A_1	Z; $f_0=X^2+Y^2$; Z^2; $f_0'=f_\alpha^2+f_\beta^2$
E_1	Y; YZ $-X$; $-ZX$
E_2	$f_\alpha=X^2-Y^2$; $f_\alpha'=f_\alpha^2-f_\beta^2$ $f_\beta=-2XY$; $f_\beta'=-2f_\alpha f_\beta$

From Eqs. (3), (6), and (8) the energy shifts are

$$\begin{aligned} \Delta E_{A_1}&=a'_{A_1}(\sigma_{xx}+\sigma_{yy})+b'_{A_1}\sigma_{zz}, \\ \Delta E_{E_1}&=a'_{E_1}(\sigma_{xx}+\sigma_{yy})+b'_{E_1}\sigma_{zz} \pm c'_{E_1}[(\sigma_{xx}-\sigma_{yy})^2+4\sigma_{xy}^2]^{1/2}, \\ \Delta E_{E_2}&=a'_{E_2}(\sigma_{xx}+\sigma_{yy})+b'_{E_2}\sigma_{zz} \pm c'_{E_2}[(\sigma_{xx}-\sigma_{yy})^2+4\sigma_{xy}^2]^{1/2}, \end{aligned} \tag{10}$$

where

$$a_i'=a_i(s_{11}+s_{12})+b_i s_{13}, \quad b_i'=2a_i s_{13}+b_i s_{33}, \quad c_i'=c_i|s_{11}-s_{12}|, \quad i=A_1,\ E_1,\ \text{or } E_2. \tag{11}$$

IV. EXPERIMENTAL RESULTS AND DISCUSSION

A. One-phonon spectrum: Zero stress

In Fig. 1 we show the entire one-phonon Raman spectrum of CdS recorded with liquid nitrogen as coolant and 5145-Å Ar$^+$ exciting radiation. In the upper-half, the right-angle scattering configuration $y'(xx+xy')z'$ selects the phonon wave vector $\vec{q}\|\hat{y}$ for which the polar phonons are E_1(TO: $\hat{x}$), E_1(LO: $\hat{y}$), and A_1(TO). In the lower-half, $\bar{y}'(xx+xy')z'$ selects $\vec{q}\|\hat{z}$ for which the polar phonons

TABLE V. Decomposition of products of basis functions of E_1 and E_2.

	(i) E_1 irreducible representation	
	X	Y
X	$\frac{1}{2}(f_0+f_\alpha)$	$-\frac{1}{2}f_\beta$
Y	$-\frac{1}{2}f_\beta$	$\frac{1}{2}(f_0-f_\alpha)$
	(ii) E_2 irreducible representation	
	f_α	f_β
f_α	$\frac{1}{2}(f_0'+f_\alpha')$	$-\frac{1}{2}f_\beta'$
f_β	$-\frac{1}{2}f_\beta'$	$\frac{1}{2}(f_0'-f_\alpha')$

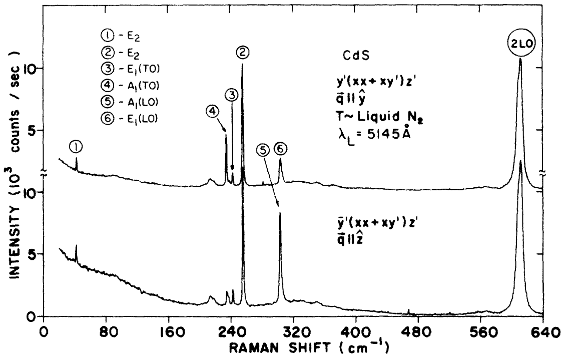

FIG. 1. Raman spectrum of CdS recorded with liquid nitrogen as coolant and excited with $\lambda_L = 5145$-Å Ar^+ radiation in the right-angle scattering geometry in the *yz* scattering plane. In the lower part of the figure the incident and scattered light are along y' and z', each 45° with respect to z, i.e., a "45° cut" sample was employed. Here $\hat{z} \parallel \vec{c}$ and $\hat{x} \parallel \vec{a}$ and the scattering geometry results in phonon wave vector $\vec{q}$ along $\hat{z}$. In the upper part the incident beam has been reversed, resulting in $\vec{q} \parallel \hat{y}$. The spectra were recorded with the incident polarization along x with no analyzer in the scattered beam.

are now $E_1(\mathrm{TO}{:}\ \hat{x})$, $E_1(\mathrm{TO}{:}\ \hat{y})$, and $A_1(\mathrm{LO})$. It should be emphasized that for $\vec{q} \parallel \hat{z}$, the E_1 is *doubly degenerate* TO whereas for $\vec{q} \parallel \hat{y}$ it suffers a LO-TO *splitting*. The two E_2 phonons, labeled (1) and (2) in the figure, are independent of phonon propagation direction and are observed in both cases. Separate polarization measurements show that they are both present for (xx), (xy'), $(z'y')$, and $(z'x)$, the four possible polarizations for this scattering configuration, in excellent agreement with the Raman tensors for an E_2 mode given in Table II. The $A_1(\mathrm{TO})$ line, labeled (4) in the figure, is observed prominently for $\vec{q} \parallel \hat{y}$ but also weakly for $\vec{q} \parallel \hat{z}$. Polarization measurements show that it is observed in (xx) and $(z'y')$ and not in (xy') and $(z'x)$, in agreement with the Raman tensor of the A_1 mode. The $A_1(\mathrm{LO})$ line, labeled (5) in the figure, is observed prominently for $\vec{q} \parallel \hat{z}$, but only weakly for $\vec{q} \parallel \hat{y}$. Polarization measurements show that the line is present in (xx) and $(z'y')$ only, also in agreement with the Raman tensor of the A_1 mode. The $E_1(\mathrm{TO})$ line, labeled (3) in the figure, is observed for both phonon directions. For $\vec{q} \parallel \hat{y}$ polarization measurements are in excellent agreement with the Raman tensor of $E_1(-X)$. The intensities of the line in (xy') and $(z'x)$ are the same as the corresponding ones for $\vec{q} \parallel \hat{z}$. However, a somewhat weaker intensity observed for it in (xx) and $(z'y')$ for $\vec{q} \parallel \hat{z}$ is not in agreement with the Raman tensors; this anomaly was not present for $\vec{q} \parallel \hat{y}$, pointing its origin to $E_1(Y)$. The $E_1(\mathrm{LO})$ line, labeled (6) in the figure, appears only for $\vec{q} \parallel \hat{y}$. Polarization measurements show that it is observed together with the $A_1(\mathrm{LO})$ line for (xx) and $(z'y')$ only, also not in agreement with its Raman tensor. The observation of the $E_1(\mathrm{LO})$ line for $y'(z'y')z'$ is equivalent to that of the forbidden $E_1(\mathrm{LO})$ in $x(zz)y$ reported by Martin and Damen[37] and by Callender *et al.*[17] who report the observation of $E_1(\mathrm{LO})$ in $x(zz)y$ as well as $x(zz)\bar{x}$. It is also interesting to note that Colwell and Klein[38] observed this line in the forbidden $y(xx)y$ and $\bar{y}(xx)y$ configurations similar to our $y'(xx)z'$ observation. The origin of the $E_1(\mathrm{TO})$ for $y'(z'y')z'$ and $y'(xx)z'$ is not clear but could also be due to resonance effects. The observation of $A_1(\mathrm{TO})$ for $\vec{q} \parallel \hat{z}$ and of $A_1(\mathrm{LO})$ for $\vec{q} \parallel \hat{y}$ is anomalous in that they should be absent for these $\vec{q}$'s; the anomaly can be ascribed to exciting radiation being reflected back from the exit face of the crystal and indeed the intensities of these forbidden lines are consistent with the reflectivity of CdS. The relatively large background even at 42 cm^{-1} from the 5145-Å laser line is reduced by a factor of 10 by using liquid-helium coolant and is believed to be due to fluorescence of the crystal.

B. One-phonon spectrum: Uniaxial stress

In Fig. 2 we show the results for $\vec{F} \parallel \hat{x}$ at a compressive stress of 2.5 kbar. The higher-frequency E_2 line at 256 cm^{-1} has been clearly split into two components. By separate polarization measurements, each component has been clearly identified from its distinct polarization features as indicated (see Table II). The neodymium calibration line allows improved accuracy in the determination of the position of each line. Figure 3 shows the Raman shift as a function of compressive stress for $\vec{F} \parallel \hat{x}$ with $\vec{q} \parallel \hat{y}$ or $\vec{q} \parallel \hat{z}$. Typical uncertainties are indicated and least-squares fits shown. Note that the E_2 doublet has been split into its clearly resolved components. Also the $E_1(\mathrm{LO})$ and $E_1(\mathrm{TO})$ lines exhibit significantly different slopes and can be viewed as a doublet separated initially by the

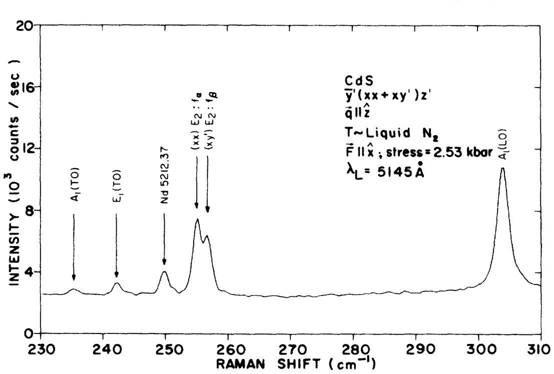

FIG. 2. Raman spectrum of CdS under a uniaxial compressive force $\vec{F}$ along $\hat{x}$. The neodymium hollow cathode lamp provided the calibration line at 5212.37 Å.

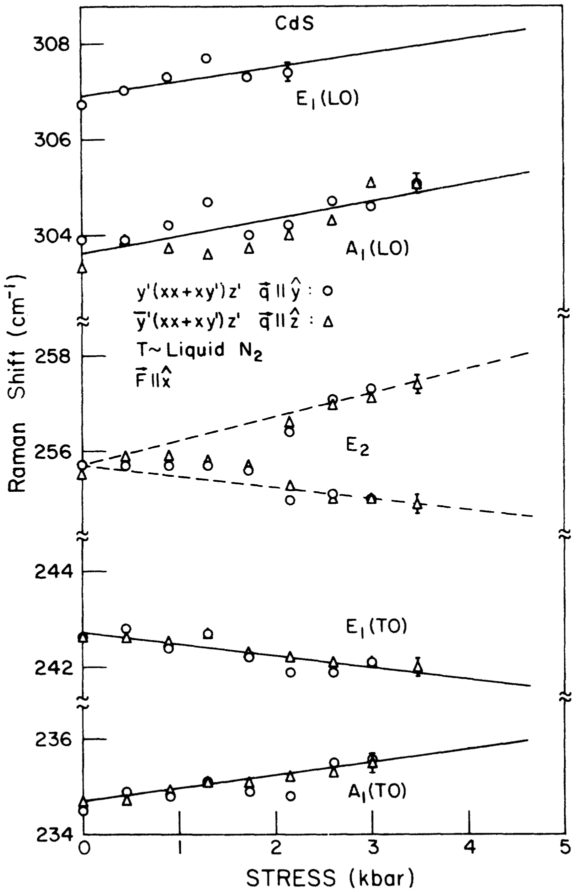

FIG. 3. Raman lines of CdS as a function of uniaxial stress with $\vec{F} \parallel \hat{x}$. The straight lines are least-squares fits. Uncertainties in the Raman shift are shown. The positions of the E_2 components for stresses below 2 kbar represent the weighted center of the two unresolved components.

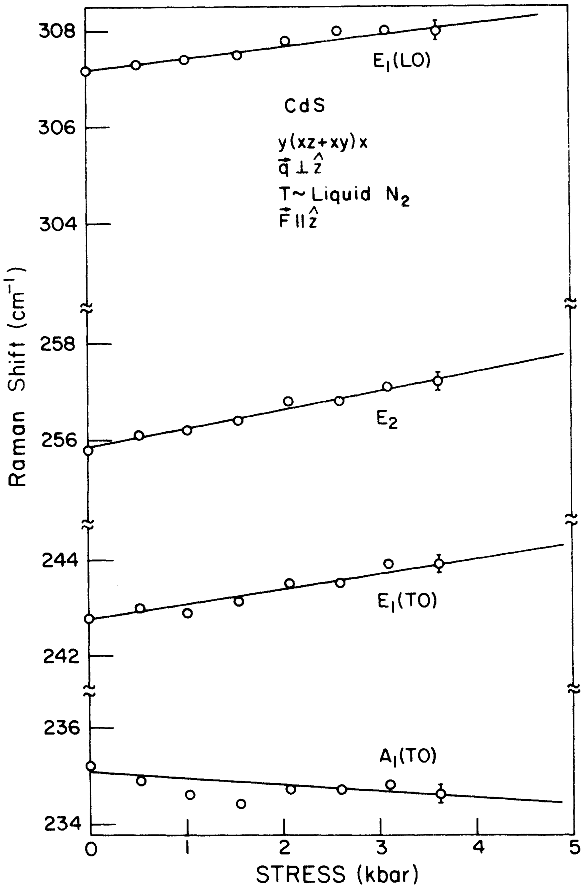

FIG. 4. Raman lines of CdS as a function of uniaxial stress with $\vec{F} \parallel \hat{z}$.

LO-TO splitting due to the long-range polarization field. We assume this LO-TO splitting to be independent of the applied stress as indicated by the A_1(LO) and A_1(TO) lines exhibiting nearly the same slope.[39] Figure 4 shows similar results for $\vec{F} \parallel \hat{z}$ with $\vec{q} \perp \hat{z}$. Here none of the lines are split, in agreement with theory. The E_1(LO) and E_1(TO) lines have essentially the same slope, in agreement with our assumption of a stress-independent LO-TO splitting.

On the basis of these results, the constants a', b', and c' for the entire one-phonon spectrum have been deduced. These, along with zero-stress line positions, are tabulated in Table VI.[40] Since the lower frequency E_2 line was not observed to split, only an upper limit is given for the magnitude of c'. As a check on these values, it is of interest to compare them with the values obtained from the room-temperature hydrostatic stress experiments carried out by Mitra and co-workers on the lower-frequency E_2 line and the E_1(LO) line.[20] For hydrostatic stress, $\sigma_{xx} = \sigma_{yy} = \sigma_{zz} = T$ and $\sigma_{xy} = \sigma_{yz} = \sigma_{zx} = 0$. Substituting these into Eqs. (10) one obtains energy shifts as

$$\Delta E_i = a_i'(\sigma_{xx} + \sigma_{yy}) + b_i'\sigma_{zz} = (2a_i' + b_i')T, \quad i = A_1,\ E_1,\ \text{or } E_2 \tag{12}$$

for all three types of phonons. As can be seen from Table VI, our calculated hydrostatic stress dependence of the Raman lines are in good agreement with those of Mitra *et al.* From the known elastic compliance constants[36] and Eq. (10), the deformation-potential constants have been calculated and are given in Table VI. For comparison, the similar constants of α-quartz are also given.

The uncertainty associated with the position of the lower frequency E_2 line results from its relatively weak intensity for 5145-Å incident radiation. As was shown by Damen and Scott,[41] by choosing somewhat shorter incident wave lengths this intensity can be increased. Under uniaxial

TABLE VI. Deformation-potential constants of CdS and α-quartz. a', b', c', d' are in cm^{-1}/kbar and a, b, c, d are in cm^{-1}/(unit strain).

Crystal	Phonon symmetry	(cm^{-1})	a'	b'	c'	d'	$2a'+b'$	$2a'+b'$ [a]	a	b	c	d
CdS [c]	E_2	41.8	0.04	0.065	0.05 [b]		0.15	0.20	~96	~104	16 [b]	
	E_2	255.7	−0.15	−0.35	0.33		0.65		−404	−483	107	
	E_1(TO)	242.6	−0.06	−0.29	0.175		−0.41	−0.43	−235	−330	57	
	E_1(LO)	306.9										
	A_1(TO)	234.7	−0.37	0.055			−0.69		−526	−328		
	A_1(LO)	303.6										
α-quartz [d]	E	128	−0.17	0	0.17	0			−218	−58	174	−160
	A_1	205	−0.74	−0.74					−814	−1000		

[a] See Ref. 20.

[b] This represents an upper limit for $|c'|$ and $|c|$ only.

[c] Errors in a', b', and c' are ±0.06 cm^{-1}/kbar.

[d] See Ref. 35.

stress for $\vec{F} \parallel \hat{x}$, however, this intensity again decreases drastically for 4880- and 4965-Å exciting radiation as shown in Fig. 5. For 5017-Å excitation the decrease is not as marked, but a very intense luminescence background arises in the region of interest; this is the so-called "blue and green emission" resulting from dislocation effects caused by the uniaxial stress.[42]

It is of interest to consider the large intensity decrease of the low-frequency E_2 line in terms of the stress induced changes in the band gap and the associated intrinsic and bound excitons. The energies of the intrinsic excitons as a function of uniaxial compression have been reported by Rowe *et al.*[43] For compressive force $\vec{F} \parallel \hat{x}$, the A-exciton energy decreases and the B- and C-exciton energies increase. Assuming the A exciton to be of dominant importance in the scattering, its decrease in energy as a result of uniaxial compression corresponds to employing a larger incident energy or shorter incident wavelength at zero stress; this assumption in turn would predict an *increase* in the intensity of the E_2 line due to a decrease in the energy denominator of the Raman cross section. In contrast, the results of Fig. 5 show a *decrease*; though this constitutes an anomaly, it is consistent with the results of Fig. 1 of Ref. 41, except that the fall off in intensity is quantitatively much too rapid when scaled according to the rates of energy shift given in Ref. 43. If the bound excitons[3] I_1 and I_2 are invoked to explain the behavior of the E_2 line under stress, with the additional assumption that they behave under stress similar to the A exciton, it is possible to understand the decrease of intensity only for the 4880-Å excitation. Similarly, it has not been possible to construct a satisfactory explanation in

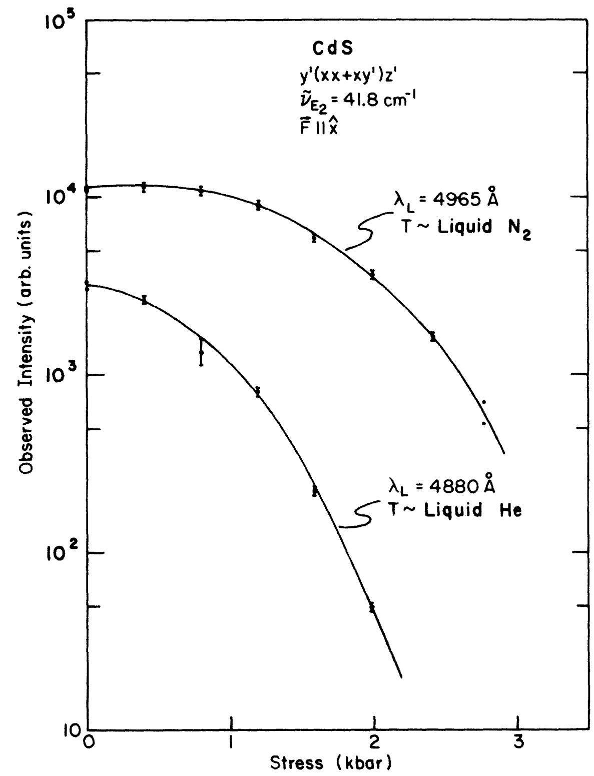

FIG. 5. Intensity of the 41.8-cm^{-1} E_2 line of CdS as a function of uniaxial stress with $\vec{F} \parallel \hat{x}$. The line was excited with 100 mW of 4965-Å Ar^+ radiation at liquid-nitrogen temperature and with 50 mW of 4880-Å Ar^+ radiation at liquid-helium temperature. The spectral slit width used in these measurements is 2 cm^{-1}. The larger uncertainty associated with the measurement at 0.8 kbar and λ_L = 4880 Å results from the Raman line being nearly coincident with the exciton luminescence.

TABLE VII. Polarizability tensors for the E modes of α-quartz.

	Rectangular cut: x, y, z	45° cut: x, y', z'
$E:X$	$\begin{pmatrix} r & 0 & 0 \\ 0 & -r & s \\ 0 & s & 0 \end{pmatrix}$	$\begin{pmatrix} r & 0 & 0 \\ 0 & -s-\frac{1}{2}r & -\frac{1}{2}r \\ 0 & -\frac{1}{2}r & s-\frac{1}{2}r \end{pmatrix}$
$E:Y$	$\begin{pmatrix} 0 & -r & -s \\ -r & 0 & 0 \\ -s & 0 & 0 \end{pmatrix}$	$\begin{pmatrix} 0 & (s-r)/\sqrt{2} & -(s+r)/\sqrt{2} \\ (s-r)/\sqrt{2} & 0 & 0 \\ -(s+r)/\sqrt{2} & 0 & 0 \end{pmatrix}$

terms of the stress-induced behavior of the B and C excitons.

C. Comparison with quartz

The point-group symmetries of CdS, α-quartz, and β-quartz, C_{6v}, D_3, and D_6, respectively, bear interesting relationships. On the one hand C_{6v} and D_6 are isomorphous and on the other D_3 is a subgroup of D_6. The Raman spectrum of α-quartz is extremely well studied both with and without uniaxial stress[35,44] and the Raman and infrared spectra of α- and β-quartz have been compared by Scott and Porto.[44] It thus appears of interest to compare our results for CdS with those for quartz.

From a comparison of the irreducible representations of C_{6v} and D_3, one notes that the polarizability tensors characterizing the E mode of D_3 are a superposition of the corresponding tensors for the E_1 and the E_2 modes of D_6. For convenience, we give the polarizability tensors for the E modes of α-quartz in Table VII. Note, however, that the $E_1(X)$ and $E_1(Y)$ of D_6 are correlated with $E_1(Y)$ and $E_1(-X)$ of C_{6v}, respectively.[45] In contrast to the E_1 components of CdS, both the $E(X)$ and $E(Y)$ components for α-quartz are allowed in the "45° cut" with $\bar{y}'(xx+xy')z'$ or $y'(xx+xy')z'$ geometries; these components occur as a doubly degenerate TO or as a LO-TO pair, respectively.

Whereas the electrostatic forces dominate over the anisotropy of interatmoic forces in all the polar modes of CdS, for α-quartz the relative strengths of the two forces depend on the particular polar mode in question. The 128-, 263-, 695-, and 1160-cm^{-1} Raman lines do not exhibit any observable LO-TO splitting and are classified as[35,46] E(LO+TO); here electrostatic effects clearly are much weaker than the anisotropy effects. For the 393–400-, 796–805-, and 450–509-cm^{-1} LO-TO doublets these two effects are comparable whereas for the 1064–1231-cm^{-1} LO-TO doublet the electrostatic effects dominate over anisotropy effects.[44,47] The four unresolved E(LO+TO) doublets have been shown to split under uniaxial stress by Tekippe *et al.*[35] For the four other LO-TO doublets, it is useful to choose the "45°-cut" and $\bar{y}'(xx+xy')z'$ and $y'(xx+xy')z'$ scattering geometries which result in $\vec{q}\parallel\hat{z}$ and $\vec{q}\parallel\hat{y}$, respectively, and allow at the same time application of $\vec{F}\parallel\hat{x}$;

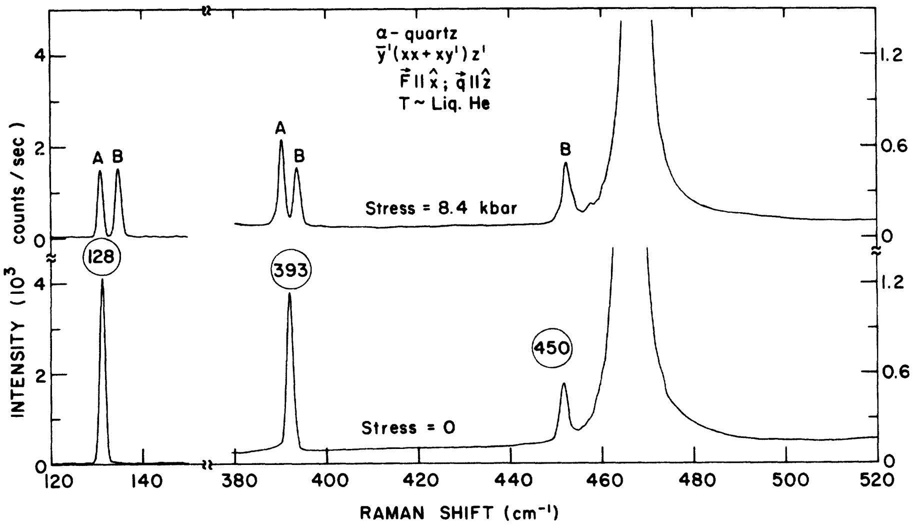

FIG. 6. Effect of uniaxial stress on the Raman lines of α-quartz having E symmetry. A "45°-cut" sample was used and liquid helium used as coolant. $\vec{F}\parallel\hat{x}$ and $\vec{q}\parallel\hat{z}$. The encircled numbers denote the zero-stress room-temperature positions of the Raman lines as given in Ref. 35.

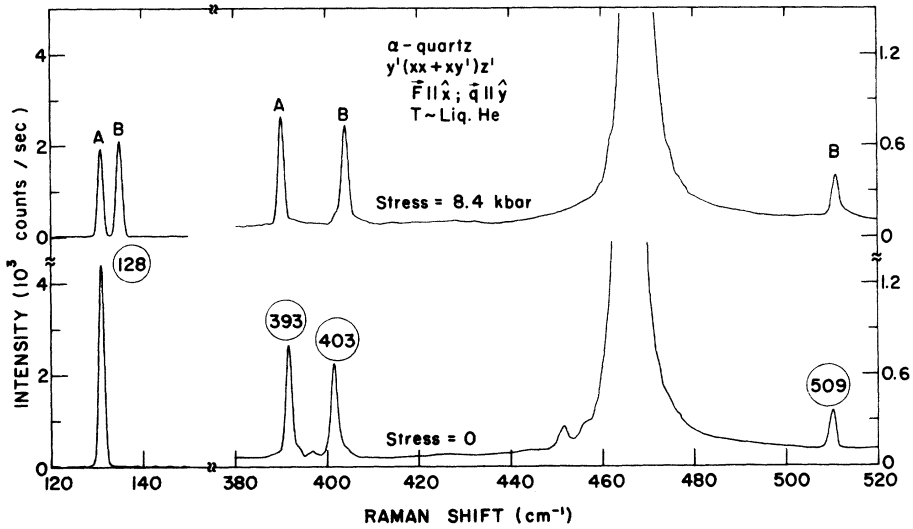

FIG. 7. Effect of uniaxial stress on the Raman lines of α-quartz having E symmetry. $\vec{F}\parallel\hat{x}$ and $\vec{q}\parallel\hat{y}$. Liquid helium used as coolant.

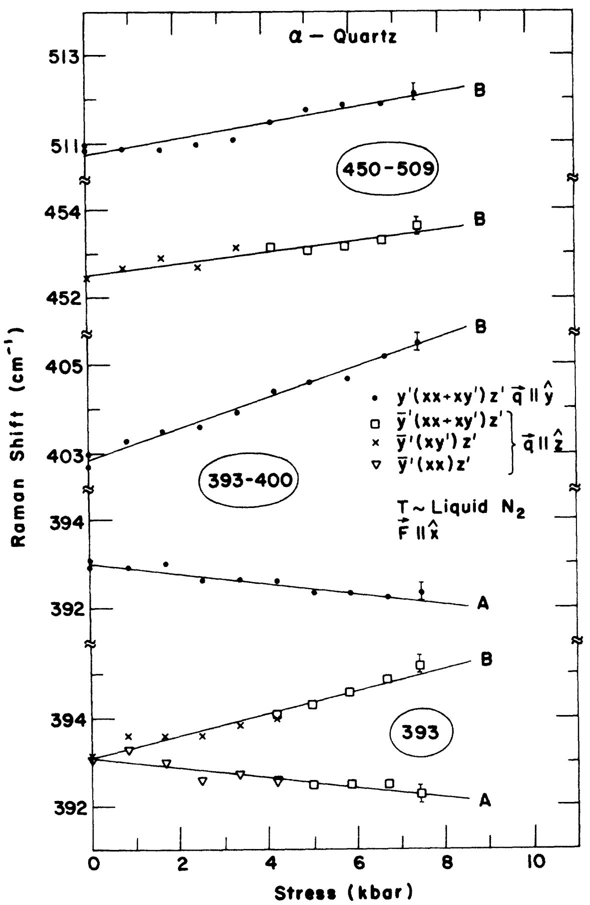

FIG. 8. Raman lines of α-quartz as a function of uniaxial stress with $\vec{F}\parallel\hat{x}$ for the geometries of Figs. 6 and 7. Typical uncertainties in line positions are indicated and the straight lines represent least-squares fits. Liquid nitrogen used as coolant.

as in the case of CdS, pure E(LO) and E(TO) components occur for both geometries.

Figure 6 shows the Raman spectrum of α-quartz recorded at liquid-helium temperature with $\bar{y}'(xx+xy')z'$ and $\vec{F}\|\hat{x}$ with $\vec{q}\|\hat{z}$ and a compressive stress of 8.4 kbar. As can be seen, the 128-cm^{-1} doublet splits into two components labeled A and B. Here A and B denote the irreducible representations of C_2, the reduced symmetry of α-quartz for $\vec{F}\|\hat{x}$ and correspond to E(TO: $\hat{x}$) and E(TO: $\hat{y}$), respectively. Similarly, the 393-cm^{-1} line splits into its A and B components as indicated. The B component of the 450-cm^{-1} TO doublet shifts to higher energy; the A component is not observed, consistent with the fact that even for $\vec{F}=0$ the 450-cm^{-1} line appears only in the (xy') polarization.

Figure 7 shows the Raman spectrum of α-quartz with $y'(xx+xy')z'$ and $\vec{F}\|\hat{x}$, for the same stress as that for Fig. 6 but now with $\vec{q}\|\hat{y}$. As can be seen the 128-cm^{-1} LO-TO doublet splits into its E(TO: $\hat{x}$) or A and its E(LO: $\hat{y}$) or B components as indicated. The corresponding A and B components of the 393-400-cm^{-1} LO-TO doublet are separated further under stress. The 509-cm^{-1} B component of the 450-509-cm^{-1} LO-TO doublet shifts to higher energy as in the other geometry. The A component expected at 450 cm^{-1} is not observed for this geometry also.

The absence of the A component of the 450-509-cm^{-1} doublet in Figs. 6 and 7 is due to the fact that the polarizability tensor component $r\sim 0$ as was shown by Scott and Porto.[44] As can be seen from Table VII, this would result in its polarizability tensor resembling that for an E_1 mode of β-quartz. In contrast to the E_1 mode of CdS

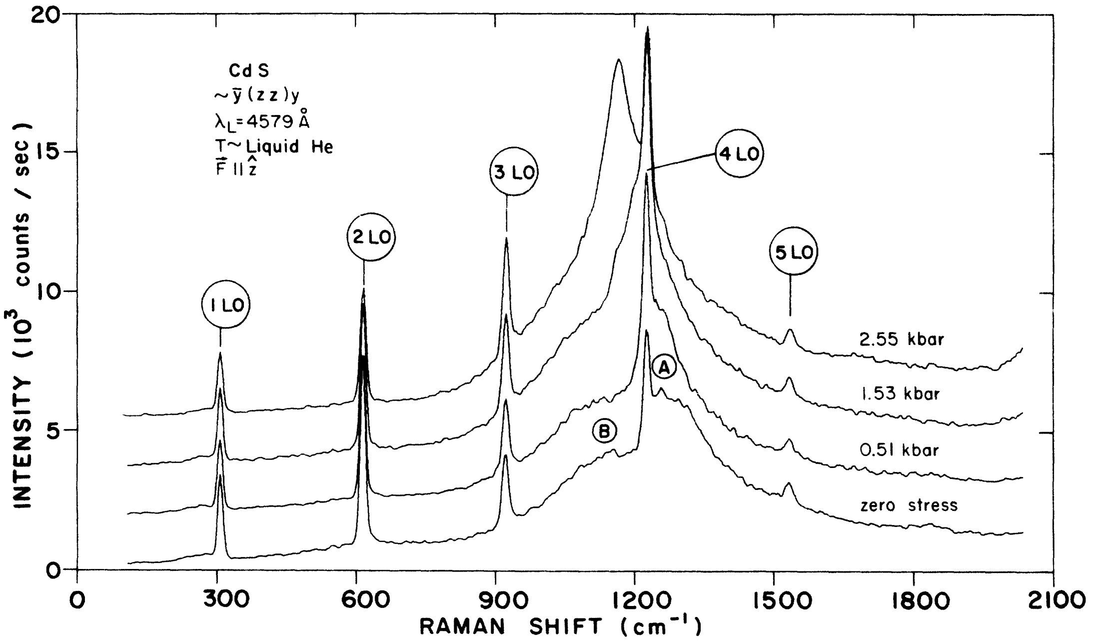

FIG. 9. Raman spectrum of CdS showing the LO overtones. $\lambda_L = 4579$-Å Ar^+ radiation having an energy well above the band gap. The spectrum was recorded in the backscattering geometry along $\hat{y}$. The incident and scattered light are polarized and analyzed parallel to $\hat{z}$. The broad features labeled A and B are due to the exciton luminescence. The various spectra show the effect of uniaxial stress with $\vec{F} \parallel \hat{z}$. Liquid helium used as coolant. For clarity, the spectra have been displaced vertically from one another.

whose allowed $E(-X)$ remains TO for both geometries, the E mode of α-quartz, allowed as $E(Y)$ only, changes from TO to LO as $\vec{q} \parallel \hat{z}$ changes to $\vec{q} \parallel y$. Although the distinction between E_1 and E_2 exists formally only for β-quartz, the E vibrations of α-quartz do show either E_1 or E_2 characteristics, viz., the 128-, 695-, 1160-, 393–400-cm^{-1} doublets show an E_2 nature and the 263-, 450–509-, and 796–805-cm^{-1} doublets show an E_1 nature.[44,48]

Figure 8 summarizes the Raman shift as a function of compressive stress for the 393–400- and the 450–509-cm^{-1} doublets with $\vec{F} \parallel \hat{x}$ in both geometries. Typical uncertainties are indicated and least-squares fits shown. As expected the 393-cm^{-1} A component exhibits the same slope for the two phonon directions. For $\vec{q} \parallel \hat{y}$, the 393-$cm^{-1}$ TO and the 403-cm^{-1} LO lines, both of B character, have nearly the same slope as can be seen. Similarly, the 450-cm^{-1} TO and 509-cm^{-1} LO, both B components, have the same slope, indicating that the polarization field causing the LO-TO splittings is relatively independent of the applied stress similar to the case of CdS. A more detailed study of the effects of uniaxial stress on the entire Raman spectrum of α-quartz is in progress.

As a result of the difference in symmetry between quartz and CdS, the energy shifts of the two components of the E modes are given by

$$\Delta E_E = a'(\sigma_{xx} + \sigma_{yy}) + b'\sigma_{zz} \pm \{[c'(\sigma_{xx} - \sigma_{yy}) + d'\sigma_{yz}]^2 + (2c'\sigma_{xy} + d'\sigma_{zx})^2\}^{1/2}. \tag{13}$$

Here, in contrast to Eq. (10), an additional constant d' occurs which is associated with the σ_{yz} and σ_{zx} components of shear stress. For $\vec{F} \parallel \hat{x}$ or $\vec{F} \parallel \hat{z}$ these shear components vanish, resulting in the energy changes being describable in terms of a', b', and c' as for CdS. It is interesting to note that this group-theoretically predicted additional constant d' was measured to be zero for the 128-cm^{-1} line of α-quartz. The deformation-potential constants are given in Table VI for comparison with CdS.

D. Overtones of A_1(LO) and E_1(LO): Effects of uniaxial stress

It is well known that CdS, when excited with laser energy close to the band gap, exhibits a series of Raman lines which are the overtones of the A_1(LO) and/or E_1(LO) fundamentals. A typical spectrum with liquid-helium coolant and 4579-Å exciting radiation is shown in Fig. 9. In addition to the overtones of various orders, labeled 1LO–5LO, one sees a relatively broad luminescence associated with the intrinsic A and B excitons nearly coincident with the 4LO; the energies of the excitons are obtained by subtracting their positions in the figure from the energy of the exciting radiation. The zero-stress exciton energies are consistent with those given by Thomas and Hopfield.[49] As pointed out by Dutton,[50] surface preparation is responsible for the large width observed for these exciton peaks. Similarly, the linewidths of the overtones are broadened by the surface polishing as reported by Damen *et al.*[51] When the Raman spectrum is excited by 4579-Å radiation the higher overtones occur in the vicinity of the A and B exciton energies resulting in the observation of a large number of overtones. In the $\sim\bar{y}(zz)y$ scattering geometry, the intense A exciton, polarized perpendicular to $\hat{z}$, does not occur and allows a convenient geometry for the observation of the overtones; the finite collection angle, however, accounts for the appearance of the A exciton in Fig. 9. It should be noted that although α_{zz} for the 1LO of E_1 symmetry vanishes according to the simple polarizability tensor characterizing it (see Table II), resonance effects allow this "forbidden" component to be observed.[17]

For $\vec{F}\parallel\hat{z}$, the exciton shifts to higher energy, seen in Fig. 9 as a smaller "Raman shift"; the stress dependence of the exciton energy agrees with that reported by Rowe *et al.*[43] who studied the effect of uniaxial stress in the reflectivity peak associated with the A exciton. For $\vec{F}\parallel\hat{z}$ all the overtones shift to higher energy, the higher-order overtones shifting faster. The rates of energy shift for each overtone are given in Fig. 10. No pronounced difference between measurements using liquid nitrogen or liquid helium as coolant was observed. Also, no difference between 4579-, 4658-, 4727-, or 4765-Å incident radiation was observed. The observed rate of shift of the 1LO line, -0.33 cm^{-1}/kbar, is close to that of the E_1 line measured from a right-angle scattering experiment (b' in Table VI). This indicates that the 1LO line is of E_1 nature and that the stress in the volume close to the surface effective in the back scattering geometry is comparable to that in the bulk material from which scattering occurs in the right-angle scattering geometry. The slope of the least-squares fit in Fig. 10, -0.229 cm^{-1}/(kbar order), strongly suggests that all the overtones are also of predominantly E_1 nature. Experiments with $\vec{F}\parallel\hat{x}$ have not yielded clear cut results; it appears that the large linewidths make observations of line splittings, expected for these overtones, difficult to observe. It would be of interest to perform experiments with cleaved samples where narrower linewidths may reduce this difficulty.

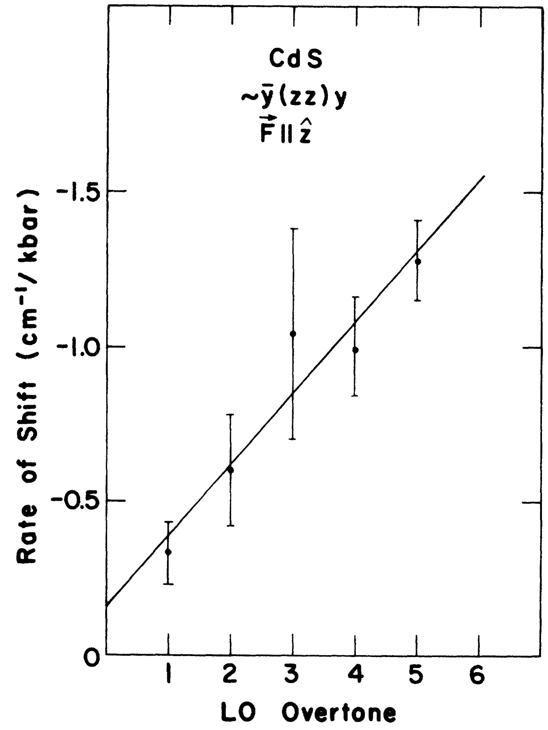

FIG. 10. Rates of shift of the LO overtones of CdS for $\vec{F}\parallel\hat{z}$. The straight line represents a least-squares fit with a slope of -0.229 ± 0.040 cm^{-1}/(kbar order).

ACKNOWLEDGMENTS

The authors wish to express their thanks to Professor S. Rodriguez, Professor B. A. Weinstein, and M. H. Grimsditch for a critical reading of the manuscript and for their comments.

---

*Work supported by the NSF Grant No. GH32001A1 and MRL Programs GH33574A1 and GH33574A3.

[1] B. Ray, *II-VI Compounds* (Pergamon, New York, 1969).

[2] Several articles in *Physics and Chemistry of II-VI Compounds*, edited by M. Aven and J. S. Prener (North-Holland, Amsterdam, 1967).

[3] D. C. Reynolds, C. W. Litton, and T. C. Collins, Phys. Status Solidi 9, 645 (1965).

[4] R. J. Collins, J. Appl. Phys. 30, 1135 (1959).

[5] A. Mitsuishi, H. Yoshinaga, K. Yata, and A. Manabe, Jpn. J. Appl. Phys. Suppl. 4, 581 (1965).

[6] H. W. Verleur and A. S. Barker, Jr., Phys. Rev. 155, 750 (1967).

[7] D. G. Thomas and J. J. Hopfield, Phys. Rev. 128, 2135

(1962).

[8] Y. S. Park and D. W. Langer, Phys. Rev. Lett. 13, 392 (1964).

[9] R. Marshall and S. S. Mitra, Phys. Rev. A 134, A1019 (1964).

[10] See S. K. Sinha, CRC Crit. Rev. Solid State Sci. 3, 273 (1973).

[11] B. Tell, T. C. Damen, and S. P. S. Porto, Phys. Rev. 144, 771 (1966).

[12] C. A. Arguello, D. L. Rousseau, and S. P. S. Porto, Phys. Rev. 181, 1351 (1969).

[13] M. A. Nusimovici and J. L. Birman, Phys. Rev. 156, 925 (1967).

[14] R. C. C. Leite and S. P. S. Porto, Phys. Rev. Lett. 17, 10 (1966).

[15] M. V. Klein and S. P. S. Porto, Phys. Rev. Lett. 22, 782 (1969).

[16] J. F. Scott, R. C. C. Leite, and T. C. Damen, Phys. Rev. 188, 1285 (1969).

[17] R. H. Callender, S. S. Sussman, M. Selders, and R. K. Chang, Phys. Rev. B 7, 3788 (1973).

[18] M. L. Shand, W. Richter, E. Burstein, and J. G. Gay, J. Nonmet. 1, 53 (1972).

[19] T. C. Damen and J. Shah, Phys. Rev. Lett. 26, 249 (1971).

[20] S. S. Mitra, O. Brafman, W. B. Daniels, and R. K. Crawford, Phys. Rev. 186, 942 (1969).

[21] A preliminary report is given in R. J. Briggs and A. K. Ramdas, Bull. Am. Phys. Soc. 20, 380 (1975).

[22] Jarrell-Ash Division, 590 Lincoln St., Waltham, Mass. 02154.

[23] RCA, Electronic Components Division, Harrison, N.J. 07029 and ITT Industrial Laboratories, Electron Tube Division, 3700 East Pontiac St., Fort Wayne, Ind. 46803.

[24] Coherent Radiation Laboratories, 3210 Porter Dr., Palo Alto, Calif. 94304.

[25] Spectra Physics, 1250 W. Middlefield Rd., Mountain View, Calif. 94042.

[26] For a complete description of the Raman spectrometer see S. Venugopalan, Ph.D. thesis (Purdue University, 1973) (unpublished).

[27] WL-22979, Westinghouse Electric Corporation, Electronic Tube Division, P. O. Box 284, Elmira, N.Y. 14902.

[28] Details of the arrangement will be given in the Ph.D. thesis of R. J. Briggs (Purdue University) (unpublished).

[29] V. J. Tekippe, Ph.D. thesis (Purdue University, 1973) (unpublished). See also V. J. Tekippe, H. R. Chandrasekhar, P. Fisher, and A. K. Ramdas, Phys. Rev. B 6, 2348 (1972).

[30] Eagle-Picher Industries, Inc., Miami Research Laboratories, P.O. Box 1090, Miami, Ok. 74354.

[31] See J. F. Nye, *Physical Properties of Crystals* (Oxford U. P., London, 1967), Appendix B, for an explanation of the Miller-Bravais coordinates; our x, y, z correspond to Nye's mutually orthogonal x_1, x_2, x_3.

[32] This enables the choice of phonon propagation to be either parallel or perpendicular to $\vec{c}$. See T. C. Damen, S. P. S. Porto, and B. Tell, Phys. Rev. 142, 570 (1966).

[33] The polishing accessories manufactured by Buehler Ltd., 2120 Greenwood St., Evanston, Ill. 60204.

[34] H. S. Peiser, J. B. Wachtman, Jr., and R. W. Dickson, J. Res. Natl. Bur. Stand. (U.S.) A 67, 395 (1963).

[35] See, for example, V. J. Tekippe, A. K. Ramdas, and S. Rodriguez, Phys. Rev. B 8, 706 (1973).

[36] D. Berlincourt, H. Jaffe, and L. R. Shiozawa, Phys. Rev. 129, 1009 (1963). We have used the elastic moduli for $T = 25$ °C determined by the extensional modes. The temperature coefficients given in this paper indicate changes in the deformation potential constants well below our experimental errors.

[37] R. M. Martin and T. C. Damen, Phys. Rev. Lett. 26, 86 (1971).

[38] P. J. Colwell and M. V. Klein, Solid State Commun. 8, 2095 (1970).

[39] A similar result was deduced for $Bi_{12}GeO_{20}$. See S. Venugopalan and A. K. Ramdas, Phys. Rev. B 8, 717 (1973).

[40] By convention compressive stress is assumed to be negative.

[41] T. C. Damen and J. F. Scott, Solid State Commun. 9, 383 (1971).

[42] H. Mitsuhashi, H. Komura, and J. Chikawa, in *II-VI Semiconducting Compounds*, edited by D. G. Thomas (Benjamin, New York, 1967), p. 179.

[43] J. E. Rowe, M. Cardona, and F. H. Pollak, in *II-VI Semiconducting Compounds*, edited by D. G. Thomas (Benjamin, New York, 1967), p. 112.

[44] J. F. Scott and S. P. S. Porto, Phys. Rev. 161, 903 (1967).

[45] The switching of the roles of X and Y results from the difference in transformation properties between σ_v of C_{6v} and C_2 of D_6.

[46] All lines are designated by their room temperature position to the nearest cm^{-1}, as given in Ref. 35 from the spectra obtained in the "rectangular cut" geometry.

[47] S. M. Shapiro and J. D. Axe, Phys. Rev. B 6, 2420 (1972).

[48] C. Y. She, J. D. Masso, and D. F. Edwards, J. Phys. Chem. Solids 32, 1887 (1971).

[49] D. G. Thomas and J. J. Hopfield, Phys. Rev. 116, 573 (1959).

[50] D. Dutton, Phys. Rev. 112, 785 (1958).

[51] T. C. Damen, R. C. C. Leite, and J. Shah, in *Proceedings of the Tenth International Conference on the Physics of Semiconductors, Cambridge, Mass., 1970*, edited by S. P. Keller, J. C. Hensel, and F. Stern (U. S. AEC, Washington, D. C., 1970), p. 735.